

# Demodulation of fiber Bragg grating sensors based on dynamic tuning of a multimode laser diode

Luís Alberto Ferreira, Evangelos Vasilios Diatzikis, Jose Luis Santos, and Faramarz Farahi

Dither demodulation of fiber Bragg grating sensors illuminated with multimode light from laser diodes is theoretically and experimentally investigated. Quasi-static temperature and strain sensitivities of  $0.09\text{ }^{\circ}\text{C}/\sqrt{\text{Hz}}$  and  $0.6\text{ }\mu\epsilon/\sqrt{\text{Hz}}$  are obtained. We show that it is possible to measure small ac signals that lie outside the feedback loop bandwidth by using a synchronous detection referenced to twice the dither frequency. In this situation, dynamic strain sensitivity of  $3.3\text{ n}\epsilon/\sqrt{\text{Hz}}$  is achieved. © 1999 Optical Society of America

OCIS codes: 060.6370, 060.2630, 350.2770.

## 1. Introduction

Fiber-sensing technology has reached qualitatively new performances with the development of fiber Bragg gratings.<sup>1-3</sup> These gratings are low-size intrinsic sensing elements that can be written in silica fibers. Since the wavelength of light is the parameter modulated by the measurand, these devices are inherently self-referenced against power fluctuations along the optical path. Also, multiplexing of these structures is conceptually simple in the wavelength domain, allowing multipoint monitoring of physical parameters, most notably strain and temperature.<sup>4</sup>

The wavelength-encoded operation of fiber Bragg gratings implies the need for efficient, versatile, and, as is desired, low-cost interrogation techniques. Toward that goal in recent years a significant number of wavelength-detection techniques for fiber Bragg grating sensors have been developed. These techniques make use of interferometric techniques,<sup>5</sup> wavelength-dependent filters,<sup>6-10</sup> tunable filters,<sup>11-13</sup> laser/sensor combinations,<sup>14,15</sup> and others.<sup>16,17</sup>

One defining factor in selection of an interrogation scheme for Bragg gratings is the spectral characteristics of the light source. Broadband optical sources such as LED, superluminescent diode, and superfluorescent devices are often used. Because of their broadband nature, the wavelength of these sources cannot be easily tuned to the Bragg wavelength.

Active tuning is a desirable approach in many cases because it not only allows in general a larger measurement range but also solves the problem of possible nonlinearity in the system transfer function. When broadband optical sources are used, active interrogation requires an external modulator such as a Fabry-Pérot interferometer,<sup>11</sup> an acousto-optic cell,<sup>18,19</sup> tunable wavelength division multiplexer,<sup>20</sup> or a tunable twin grating.<sup>12</sup> It is therefore desirable to develop a signal-processing scheme that allows active wavelength tuning of the optical source to the Bragg wavelength through direct modulation of the spectral profile of the light source. This concept has been demonstrated by use of a semiconductor distributed feedback laser as the optical source.<sup>21,22</sup> However, there are problems associated with distributed feedback lasers such as their limited tuning range and relatively high cost. The authors have researched the use of low-cost multimode laser diodes to perform the active tuning of fiber Bragg grating sensors. The results from using serrodyne frequency modulation of the multimode spectrum proved the feasibility of the concept.<sup>23</sup> Later the research progressed toward utilization of several laser modes to obtain an increased measurement range of the order of  $5\text{ m}\epsilon$  with a minimum detectable static strain of  $\sim 0.1\text{ }\mu\epsilon/\sqrt{\text{Hz}}$ .<sup>24</sup>

---

L. A. Ferreira and J. L. Santos are with Unidade de Tecnologia Optoelectrónica e Electrónica, Instituto de Engenharia de Sistemas e Computadores, Porto, Portugal. J. L. Santos is also with the Departamento de Física da Faculdade de Ciências da Universidade do Porto, Rua do Campo Alegre, 687, 4169-007 Porto, Portugal. E. V. Diatzikis and F. Farahi are with the Department of Physics, University of North Carolina at Charlotte, Charlotte, North Carolina 28223.

Received 9 December 1998; revised manuscript received 4 May 1999.

0003-6935/99/224751-09\$15.00/0

© 1999 Optical Society of America

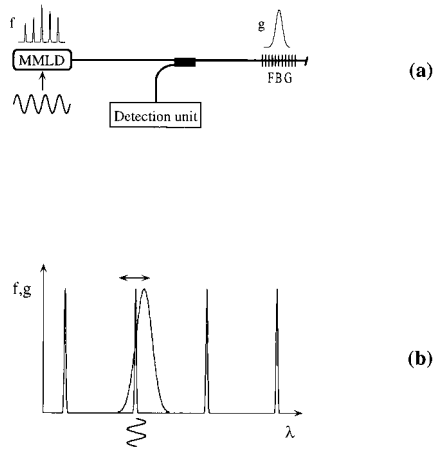


Fig. 1. Proposed scheme for fiber Bragg grating demodulation: (a) basic optical configuration: MMLD, multimode laser diode; FBG, fiber Bragg grating. (b) grating and laser spectral functions.

Fiber Bragg grating interrogation based on frequency modulation of the laser-diode light source requires a minimum number of components when compared with those using external tuning of the wavelength. In addition, this technique provides a higher-frequency modulation bandwidth. This characteristic is important when fiber gratings are used to detect relatively fast ac signals, for example, acoustic signals that are in the kilohertz range. For these cases the carrier generated by the serrodyne technique should exceed 10 kHz, which means that the flyback of the sawtooth waveform applied to the laser-diode injection current should last less than 5  $\mu$ s (5% of the total period) for the generated carrier not corrupted by significant distortion. This corresponds to a frequency-modulation bandwidth of the order of 200 kHz, which in many cases can be hard to achieve.

Fiber Bragg grating interrogation based on the sinusoidal dither approach overcomes the problem described above, basically because the sawtooth waveform required for the serrodyne technique is replaced by a sine-wave modulation.<sup>21,25-28</sup> The research presented in this paper applies the dither scheme to the sensing system of a fiber Bragg grating illuminated by a multimode laser diode. A theoretical model is developed and experimental results are presented. Also, in Section 4 a process is described to detect signals outside the bandwidth of the active tracking loop that are not observable by the conventional dither approach.

## 2. Principle

Consider the schematic of an optical sensing system illuminated by the multimode laser diode shown in Fig. 1. If one of the laser modes coincides within the spectrum of the fiber Bragg grating, reflected light associated with that laser mode will be detected at the output. The intensity of the signal at the detector is proportional to the overlap integral of the func-

tions  $f(\lambda - \lambda_0)$  and  $g(\lambda - \lambda_B)$ , representing the spectral characteristics of the laser mode and the fiber Bragg grating, respectively. Assuming that both functions are Gaussian, we can write

$$f(\lambda - \lambda_0) = \frac{2P_0}{\Delta\lambda_m} \left(\frac{\ln 2}{\pi}\right)^{1/2} \exp\left[-4 \ln 2 \left(\frac{\lambda - \lambda_0}{\Delta\lambda_m}\right)^2\right], \quad (1)$$

$$g(\lambda - \lambda_B) = R \exp\left[-4 \ln 2 \left(\frac{\lambda - \lambda_B}{\Delta\lambda_B}\right)^2\right], \quad (2)$$

where  $P_0$  is the optical power of the laser mode being reflected by the grating,  $\Delta\lambda_m$  is the mode spectral width at half-maximum, and  $\lambda_0$  is the mode central wavelength;  $R$  is the grating maximum reflectivity ( $0 \leq R \leq 1$ ),  $\lambda_B$  is the Bragg wavelength, and  $\Delta\lambda_B$  is the grating spectral width at half-maximum. The intensity of the signal at the detector can thus be written as (assuming a nominal coupling factor of 1/2)

$$I_{\text{OUT}} = \frac{1}{4} \int_0^\infty f(\lambda - \lambda_0)g(\lambda - \lambda_B)d\lambda. \quad (3)$$

In general the spectral width of the grating  $\Delta\lambda_B$  is much larger than the spectral width of the laser mode  $\Delta\lambda_m$ , and the above integral becomes

$$I_{\text{OUT}}(\Delta\lambda) \approx \frac{1}{4} P_0 R \exp\left[-4 \ln 2 \left(\frac{\Delta\lambda}{\Delta\lambda_B}\right)^2\right], \quad (4)$$

where  $\Delta\lambda = \lambda_0 - \lambda_B$  is the difference between the fiber grating and the laser-mode central wavelengths. In deriving Eq. (4), we assumed that the laser-mode separation is larger than the grating spectral width, ensuring reflection of only one mode from the grating. We shall see in Section 3 that this is a valid assumption for practical components such as those used in our experiments.

By dithering the laser with a small-amplitude sinusoidal waveform, a time-dependent change in the central wavelength of the laser mode can be produced. In this case  $\Delta\lambda$  becomes a function of time:

$$\begin{aligned} \Delta\lambda(t) &= \lambda_0(t) - \lambda_B \\ &= \overline{\lambda_0} + \Delta\lambda_0 \sin \omega t - \lambda_B \\ &= \overline{\Delta\lambda} + \Delta\lambda_0 \sin \omega t. \end{aligned} \quad (5)$$

In the above equations  $\Delta\lambda_0$  is the amplitude of the wavelength modulation,  $\overline{\Delta\lambda}$  represents the average difference between the mode central wavelength  $\lambda_0$  and the Bragg wavelength, and  $\omega$  is the frequency of the dithering signal. If we use this expression for  $\Delta\lambda$  in approximation (4), we will have an output signal that can be written as

$$\begin{aligned} I_{\text{OUT}}(\overline{\Delta\lambda} + \Delta\lambda_0 \sin \omega t) &\approx \frac{1}{4} P_0 R \\ &\times \exp\left[-4 \ln 2 \left(\frac{\overline{\Delta\lambda} + \Delta\lambda_0 \sin \omega t}{\Delta\lambda_B}\right)^2\right]. \end{aligned} \quad (6)$$

Below we demonstrate that to establish a feedback loop able to lock the laser mode to the Bragg wavelength by keeping  $\overline{\Delta\lambda}$  fixed, the component of the detected signal at the dither frequency (first harmonic) must be used. To obtain an expression for this component, one can use the Taylor series expansion of approximation (6) when term  $\Delta\lambda_0 \sin \omega t$  is treated as a perturbation around the average value  $\overline{\Delta\lambda}$ . This treatment is valid since in general the dither amplitude is small. By considering terms only as great as  $\Delta\lambda_0^4$  in the Taylor expansion of  $I_{\text{OUT}}$  at frequency  $\omega$ , we get

$$\begin{aligned}
 I^\omega(\overline{\Delta\lambda} + \Delta\lambda_0 \sin \omega t) &\approx \left. \frac{\partial I_{\text{OUT}}(\overline{\Delta\lambda})}{\partial \overline{\Delta\lambda}} \right|_{\overline{\Delta\lambda}=\overline{\Delta\lambda}} \Delta\lambda_0 \sin \omega t \\
 &+ 6P_0R \left( \frac{\ln 2}{\Delta\lambda_B^2} \right)^2 \overline{\Delta\lambda} \Delta\lambda_0^3 \left( 1 - \frac{8 \ln 2}{3\Delta\lambda_B^2} \overline{\Delta\lambda}^2 \right) \\
 &\times \exp \left[ -4 \ln 2 \left( \frac{\overline{\Delta\lambda}}{\Delta\lambda_B} \right)^2 \right] \sin \omega t = P_0R \frac{\ln 2}{\Delta\lambda_B^2} \overline{\Delta\lambda} \Delta\lambda_0 \\
 &\times \left[ -2 + \frac{6 \ln 2}{\Delta\lambda_B^2} \overline{\Delta\lambda}^2 - \left( \frac{4 \ln 2}{\Delta\lambda_B^2} \right)^2 \overline{\Delta\lambda}^2 \Delta\lambda_0^2 \right] \\
 &\times \exp \left[ -4 \ln 2 \left( \frac{\overline{\Delta\lambda}}{\Delta\lambda_B} \right)^2 \right] \sin \omega t. \quad (7)
 \end{aligned}$$

Equation (7) vanishes when  $\overline{\Delta\lambda} = 0$ , indicating that condition  $\lambda_0 = \lambda_B$  provides a suitable point for closed-loop operation. To maximize the sensitivity in measuring Bragg wavelength changes, it is important to find a value for the dither amplitude  $\Delta\lambda_0$  that maximizes the slope of the amplitude of  $I^\omega$  around  $\overline{\Delta\lambda} = 0$ . Approximation (7) indicates that the amplitude of  $I^\omega$  has a behavior approximately described by the first derivative of  $I_{\text{OUT}}$  plus a corrective term. This term allows one to obtain an optimum value for the dither modulation amplitude. Without it, the slope of the amplitude of  $I^\omega$  would increase proportionally with the dither amplitude, which is obviously incorrect.

The value of the dither amplitude that maximizes the sensitivity at the lock point,  $\overline{\Delta\lambda} = 0$ , must satisfy

$$\left. \frac{\partial}{\partial \Delta\lambda_0} \left[ \frac{\partial A^\omega(\overline{\Delta\lambda}, \Delta\lambda_0)}{\partial \overline{\Delta\lambda}} \right] \right|_{\overline{\Delta\lambda}=0} = 0, \quad (8)$$

where  $A^\omega(\overline{\Delta\lambda}, \Delta\lambda_0)$  is the amplitude of the sine wave given by approximation (7). The optimum dither amplitude is then

$$\Delta\lambda_0^{\text{opt}} = \left( \frac{\Delta\lambda_B^2}{9 \ln 2} \right)^{1/2} \approx 0.40 \Delta\lambda_B. \quad (9)$$

This result is illustrated in Fig. 2 where the dependence of  $A^\omega(\overline{\Delta\lambda}, \Delta\lambda_0)$  on the Bragg wavelength is analyzed for different values of the dither amplitude:  $0.5\Delta\lambda_0^{\text{opt}}$ ,  $\Delta\lambda_0^{\text{opt}}$ , and  $1.5\Delta\lambda_0^{\text{opt}}$ . A similar result was obtained by Xu *et al.* for a square-wave dither modulation.<sup>19</sup>

The expressions derived here are valid assuming that the dither amplitude is small. We now consider

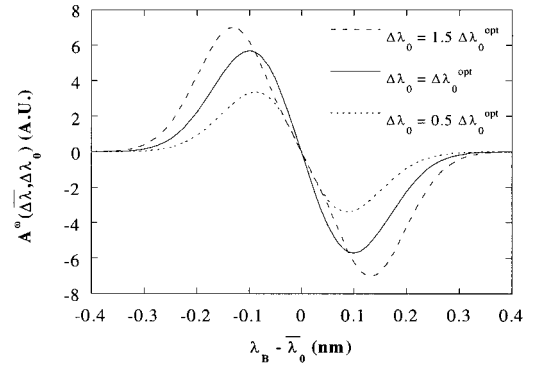


Fig. 2. First harmonic amplitude of the output signal determined by using Taylor's expansion as a function of the Bragg wavelength and for different dithering amplitudes.

the Fourier series as an alternative way to extract the first harmonic of the signal given by approximation (6) and confirm the obtained value for  $\Delta\lambda_0^{\text{opt}}$  [Eq. (9)]. To obtain an analytical solution, we need some approximations that have the same implications as those considered above. However, numerical analysis involving the Fourier term at frequency  $\omega$  can be performed that leads to a more precise solution. The first harmonic taken from the signal in approximation (6) can be written as

$$I^\omega(\overline{\Delta\lambda} + \Delta\lambda_0 \sin \omega t) = A \cos(\omega t - \theta), \quad (10)$$

where  $A$  and  $\theta$  are now Fourier coefficients, given by

$$A = (a_1^2 + a_2^2)^{1/2}, \quad (11)$$

$$\theta = \tan^{-1} \left( \frac{a_2}{a_1} \right), \quad (12)$$

where

$$\begin{aligned}
 a_1 &= \frac{2}{T} \int_0^T I_{\text{OUT}}(\overline{\Delta\lambda} + \Delta\lambda_0 \sin \omega t) \cos \omega t dt, \\
 a_2 &= \frac{2}{T} \int_0^T I_{\text{OUT}}(\overline{\Delta\lambda} + \Delta\lambda_0 \sin \omega t) \sin \omega t dt. \quad (13)
 \end{aligned}$$

In a closed-loop operation the signal of interest  $A^\omega(\overline{\Delta\lambda}, \Delta\lambda_0)$  combines parameters  $A$  and  $\theta$  from Eq. (10) in the form

$$A^\omega(\overline{\Delta\lambda}, \Delta\lambda_0) = A \sin(\pi + \theta). \quad (14)$$

Function  $A^\omega(\overline{\Delta\lambda}, \Delta\lambda_0)$  is represented in Fig. 3 for three different values of  $\Delta\lambda_0$ :  $0.6\Delta\lambda_0^{\text{opt}}$ ,  $\Delta\lambda_0^{\text{opt}}$ , and  $1.4\Delta\lambda_0^{\text{opt}}$ . Here  $\Delta\lambda_0^{\text{opt}}$  is the value that maximizes the slope of the function given by Eq. (14) at  $\overline{\Delta\lambda} = 0$  and was evaluated by such numerical methods as

$$\Delta\lambda_0^{\text{opt}} \approx 0.51 \Delta\lambda_B. \quad (15)$$

This result is not significantly different from that given by Eq. (9), showing that the analytical expressions obtained with Taylor's expansion are valid.

As shown by approximation (6) the system output

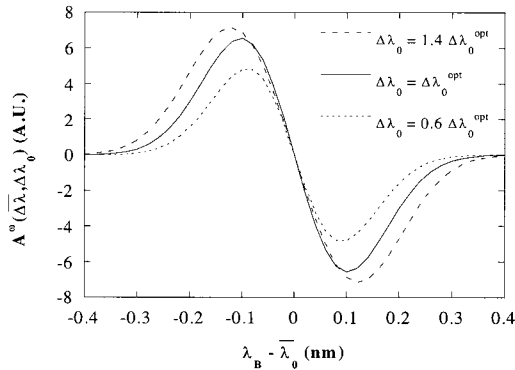


Fig. 3. First harmonic amplitude of the output signal determined by using the Fourier's series as a function of the Bragg wavelength and for different dithering amplitudes.

is a periodic function of time, and therefore its component at frequency  $\omega$  is given exactly by the first harmonic of the corresponding Fourier expansion. Actually it is the amplitude of this component that is provided by a lock-in amplifier when referenced to  $\omega$ . The analytical determination of this amplitude is not straightforward but, as shown above, a numerical evaluation can be implemented. The reason for applying a Taylor expansion to the function given by approximation (6) resulted from the fact that this expansion is based on function derivatives, directly pointing out the behavior of the amplitude of  $I^\omega$ , which is close to the first derivative of the grating spectral function. Also, it allows us to quantify in first order the corresponding deviation.

In Section 3, experimental results are presented to demonstrate the interrogation of a fiber Bragg grating sensor illuminated with a multimode laser diode by using the dither technique described here.

### 3. Experiments and Results

Figure 4 shows the experimental setup. A pigtailed multimode laser diode (Fujitsu FLD130C2LK/352) operating at 1318 nm (the wavelength of the central mode) was used to illuminate the sensing fiber Bragg grating through a 3-dB coupler,  $C_1$ . The separation between adjacent longitudinal modes of the laser was measured to be  $\sim 0.75$  nm. The temperature was tuned and the bias current was adjusted so that one

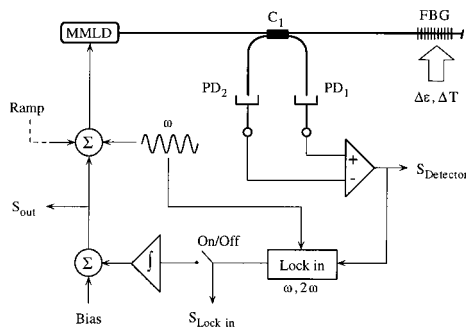


Fig. 4. Experimental arrangement for fiber Bragg grating sensor interrogation: PD, photodiode.

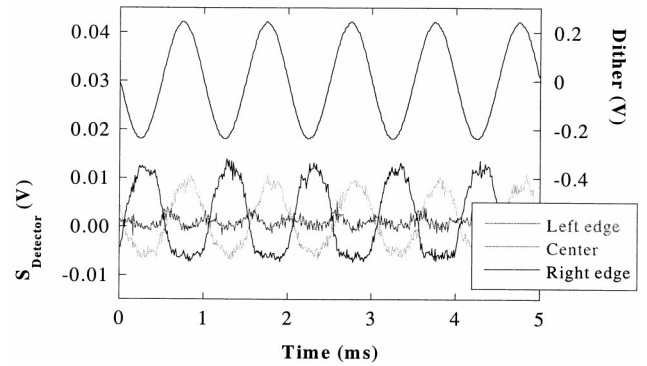


Fig. 5. Dither and detector signals for three different positions of the laser mode relative to the fiber Bragg grating spectrum (dc components removed).

of the lateral modes coincided with the fiber grating. The current-tuning capability of the laser was 11.3 pm/mA. A sinusoidal current signal with an amplitude of 1.95 mA and a frequency of 1 kHz was added to the laser bias current to dither the laser-mode wavelength. The spectral characteristics of the grating were analyzed at room temperature, and with no applied axial strain we recorded a reflectivity of  $\sim 60\%$  at  $\lambda_B = 1304.4$  nm and  $\Delta\lambda_B < 0.2$  nm. Reflected light from the grating was sent to the detection unit through coupler  $C_1$ . Spurious reflection along the optical system was minimized by applying index-matching gel to the fiber ends, and light coming directly from the laser to the coupler output was used to compensate the effect of intensity modulation of the light injected into the system. This intensity modulation comes from the unavoidable residual fraction of the entire laser spectrum reflected at the fiber ends and spliced points. The effect of this intensity modulation is to introduce measurement errors that can be important, considering that its strength can be comparable with or even higher than the signal power that comes only from the laser mode reflected by the grating. Here we should emphasize that this broadband intensity modulation does not depend on grating position.

A typical signal output as seen in the oscilloscope (with the dc component removed) is given in Fig. 5 (open loop) for three different positions of the laser mode relative to the Bragg grating: laser mode on the left edge, on the center, and on the right edge of the grating. It can be seen that when the phase of the signal is taken into account the amplitude follows a derivativelike behavior. To extract this complex amplitude, a lock-in amplifier referenced to the dither frequency was used.

A sawtooth waveform with low frequency (10 Hz) and large amplitude (62.4 mA) was added to the dither and bias signals to sweep the laser mode over the grating spectrum. This enables us to obtain at the lock-in output a periodic function with the behavior as predicted in Section 2 (Fig. 6). Simultaneously, at the detector, the signal corresponding to the laser-mode sweep over the grating is observable.

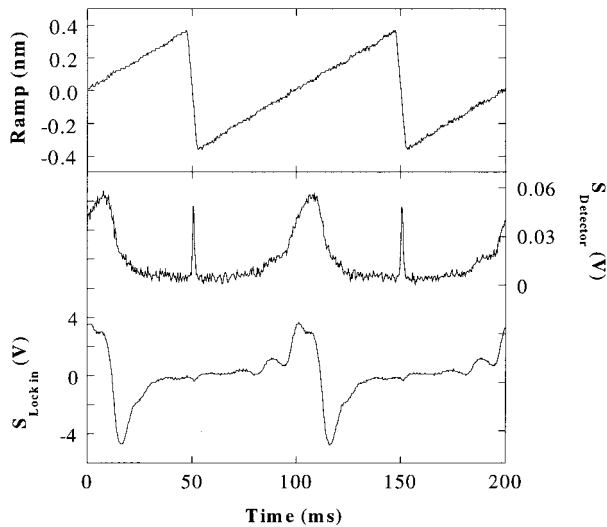


Fig. 6. Grating spectral function obtained at the detector output (middle trace) and corresponding lock-in output referenced to the dither frequency (bottom trace) when the laser mode is ramped (upper trace).

Note that, since the laser-mode spectral width is much smaller than the grating width, sweeping the grating spectrum with the laser mode reveals the spectral structure of the fiber grating with a resolution dictated by the laser-mode width. This structure is also responsible for the nonuniform behavior of the lock-in output signal. We now present results corresponding to the closed-loop operation, obtained with the ramp modulation off.

An error signal was generated by integrating the output signal from the lock-in amplifier (Fig. 4) and was added to the dither and bias signals in a feedback loop to lock the laser mode to the Bragg grating. In this case the lock-in output will always be zero, but, by monitoring the laser bias current, we can measure the change in Bragg wavelength and obtain information about the measurand status. Figure 7 illustrates the effectiveness of the servo in maintaining the lock-in output at zero value.

To evaluate the system bandwidth, a sinusoidal signal with a small amplitude was added to the laser-

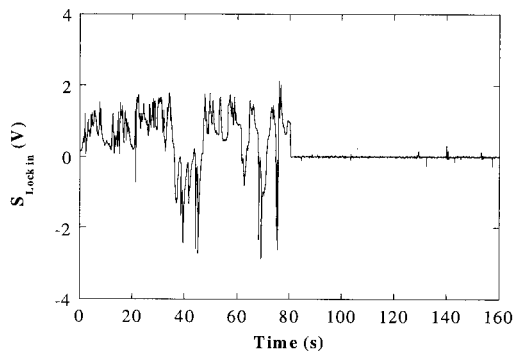


Fig. 7. Servo's effectiveness: lock-in output when the sensor head is subjected to abrupt temperature and strain variations. (For  $t < 80$  s the servo is off; for  $t \geq 80$  s the servo is on.)

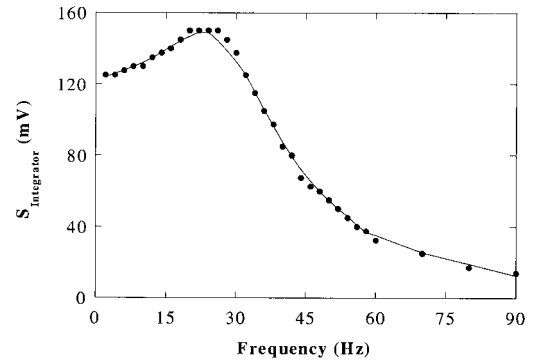


Fig. 8. System-frequency response.

diode injection current. With the loop closed and without strain or temperature applied to the grating, the integrator output (error signal) was observed as a function of frequency. The result is presented in Fig. 8 and indicates a bandwidth of  $\sim 38$  Hz. This value can be controlled by the lock-in time constant.

Figures 9 and 10 show the system response to temperature across a range of  $43^\circ\text{C}$  (Fig. 9), corresponding to a Bragg-wavelength shift of  $0.35$  nm, and to applied strain across a range of  $665 \mu\epsilon$  (Fig. 10), corresponding to a Bragg-wavelength shift of  $0.55$  nm. Data in these figures indicate linear behavior. From the spread of the data and the bandwidth of the feedback loop, sensitivities of  $0.09^\circ\text{C}/\sqrt{\text{Hz}}$  for temperature measurements and  $0.6 \mu\epsilon/\sqrt{\text{Hz}}$  for strain

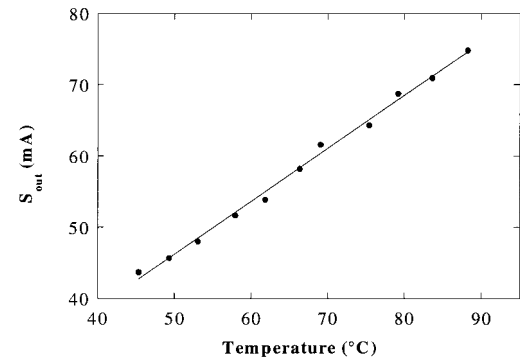


Fig. 9. System response to temperature change.

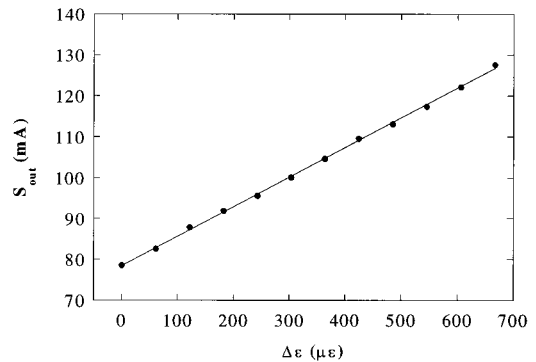


Fig. 10. System response to applied strain.

measurements were obtained. The measured sensitivity values are determined by the noise level in the system and slopes of the linear dependence between applied strain and temperature and the corresponding changes at the lock-in output, which, for a fixed dither modulation amplitude, depend only on the power level reaching the detector and grating spectral width.

The measurement range of this system is limited by the maximum current that can be applied to the laser diode. In our experiments, dynamic ranges of ~54 and ~61 dB were obtained for temperature and strain measurements, respectively. One advantage of using a multimode laser over a single-mode laser is the possibility of switching between adjacent modes to track the fiber Bragg grating while keeping the bias current within a safe limit. This capability has been experimentally demonstrated by using the serrodyne method described in Ref. 23 and 24, allowing a substantial increase in the measurement range. Another significant advantage of using a multimode laser diode rather than a single-mode laser diode is that optical isolation is not required. It was found that the lateral modes of the laser spectrum were stable even in the presence of strong back reflection, which has a significant effect in the central modes. On the other hand, the power of the lateral modes is much less than the central modes. However, because the laser mode width is much smaller than the grating spectral width, the average return power reflected by the grating is still comparable with the situation in which the fiber grating is illuminated by a broadband source. Additional advantages of this technique are its potential to be applied in multiplexed sensing and the use of low-cost light sources.

#### 4. Synchronous Detection at Double Dither Frequency

In Section 3, results for dc temperature and strain variations were presented. We now examine the application of this technique for measurement of ac strain signals with small amplitude. If the frequency of these signals is within the bandwidth of the feedback loop, information about the grating status can be obtained from the total bias current, as described above. However, in some applications fiber Bragg grating sensors are used for detection of relatively fast ac signals, with frequency beyond the bandwidth of the servo. In this case it is usual to extract the measurand information directly from the signal at the detector output. However, when the laser-mode wavelength is locked to the Bragg grating peak wavelength, the overlap integral corresponding to the laser-mode and grating spectral functions has no sensitivity to Bragg-wavelength changes, as can be verified from Eq. (4) by making  $\Delta\lambda \rightarrow 0$ . It is clear that maximum sensitivity corresponds to the situation in which the laser-mode wavelength is tuned to the inflection point in one of the grating edges.<sup>29</sup> Figure 11 illustrates the situation. We now show that, when the component of the returned signal from the grating at frequency  $2\omega$  (second harmonic) is used, it is possible to use the dither technique to lock

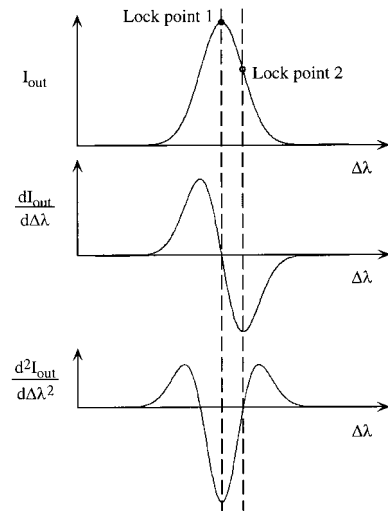


Fig. 11. Servo operation when  $\omega$  (lock point 1) or  $2\omega$  (lock point 2) is used as a reference for the lock-in amplifier.

the laser-mode wavelength to one of the fiber grating edges and measure Bragg wavelength shifts with high sensitivity at detector output.

To obtain an analytical expression for the second harmonic amplitude, we use the Taylor expansion of Eq. (6) and extract the contributions at double frequency. When only the terms containing  $\Delta\lambda_0$  and  $\Delta\lambda_0^2$  are considered, the result is

$$I^{2\omega}(\overline{\Delta\lambda} + \Delta\lambda_0 \sin \omega t) \approx - \left. \frac{\partial^2 I_{\text{OUT}}(\Delta\lambda)}{\partial \Delta\lambda^2} \right|_{\Delta\lambda = \overline{\Delta\lambda}} \frac{\Delta\lambda_0^2}{8} \times \cos(2\omega t) = P_0 R \frac{\ln 2}{\Delta\lambda_B^2} \Delta\lambda_0^2 \left( - \frac{2 \ln 2}{\Delta\lambda_B^2} \overline{\Delta\lambda}^2 + \frac{1}{4} \right) \times \exp \left[ -4 \ln 2 \left( \frac{\Delta\lambda}{\Delta\lambda_B} \right)^2 \right] \cos(2\omega t). \quad (16)$$

This result confirms that it is possible to use the second harmonic to lock the laser mode to one of the grating edges, because its amplitude is proportional to the second derivative of the grating spectral function (Fig. 11). Further refinements to Eq. (16) can again be made by considering terms containing  $\Delta\lambda_0^3$  and  $\Delta\lambda_0^4$  in Taylor's expansion. This, however, is not necessary since maximum sensitivity to Bragg wavelength shifts measured at the detector output depends mainly on the grating slope at the inflection point, which is related with its reflectivity and bandwidth. Maximization of the slope in zero crossings of the second derivative function is not mandatory here because it affects only the loop gain and therefore its stability.

We now present experimental results from using the scheme described above when ac signals that are outside the loop bandwidth were applied to the grating. The differences between this method and the one described in Section 3 are as follows: The lock-in amplifier must now be referenced to  $2\omega$ , where

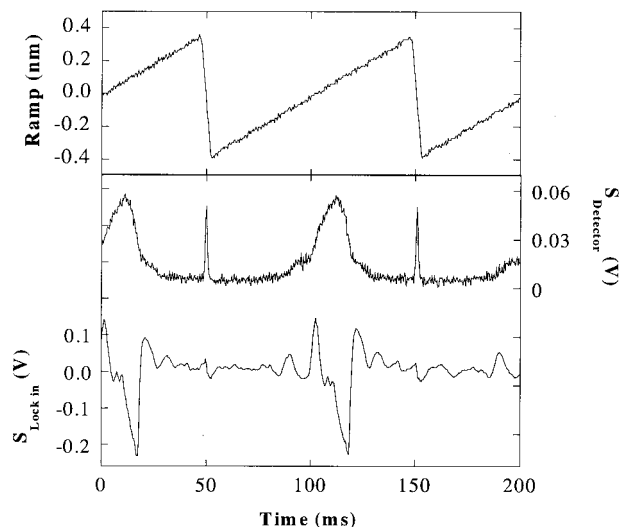


Fig. 12. Grating spectral function obtained at the detector output (middle trace) and corresponding lock-in output referenced to double the dither frequency (bottom trace) when the laser mode is ramped (upper trace).

$\omega$  is the frequency of the dithering signal; signals to be measured must be obtained at the detector output.

To demonstrate that the lock-in output can generate a second derivativelike function when referenced to  $2\omega$ , the ramp signal that we referred to in Section 3 was again utilized in open-loop operation. All other experimental conditions are the same as before. Figure 12 shows the obtained lock-in signal together with the ramp modulation and the grating spectral response as obtained at the detector output. Once again, the effect of the grating nonuniform spectral structure on the signals is apparent. Nevertheless there are two clear zero-crossing points in the lock-in signal that can be used for closed-loop operation. From Fig. 12 we can see that the zero crossing that corresponds to the right edge of the grating is the most favorable to be chosen. After the ramp modulation was disconnected, one of the laser modes was moved to the desired grating region by acting on the laser bias current and the servo was turned on.

An ac strain signal with a frequency of 200 Hz was applied to the sensing-fiber Bragg grating by using a piezoelectric transducer. The signal at the detector output was then sent to a spectrum analyzer, and the result in Fig. 13 was observed. As we predicted above, when the system is locked at the grating edge (lock point 2 in Fig. 11), the component at the dither frequency is maximized and the component at double frequency is strongly attenuated. Simultaneously a strong signal corresponding to the ac strain signal appears at the baseband, which was expected since the grating edge is a high-sensitivity point for modulation of the intensity arriving at the detector. We can also see that there are no sidebands around the strong component at  $\omega$ , whereas some small sidebands can be observed around the reduced  $2\omega$  component. In Fig. 11 we clarify these features. The

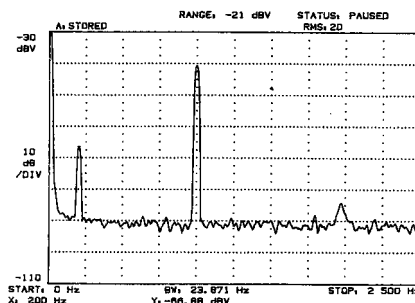


Fig. 13. Frequency spectrum of the detector output for synchronous detection at  $2\omega$  and small-amplitude strain signal applied to the fiber Bragg grating (200 Hz).

servo forces the first harmonic amplitude to be at its maximum value, therefore exhibiting very low sensitivity to amplitude modulation. On the contrary, the second harmonic amplitude is forced by the servo to be zero. Since the system is in a region of high sensitivity for the second derivative of the intensity function, any perturbation (in this case the applied strain signal) disturbs the system away from the operation point (lock point 2 in Fig. 11) and generates a signal at frequency  $2\omega$  and at its sidebands.

We can now compare this result with the one obtained when the lock-in amplifier was referenced to the dither frequency and the laser-mode wavelength was locked to the grating maximum reflectivity point (Section 3). Figure 14 shows the spectrum analyzer trace corresponding to the detector signal. Once again, Fig. 11 can be used to analyze these results. Within the loop bandwidth the amplitude of the first harmonic is always zero. Nevertheless this amplitude exhibits high sensitivity to variations in  $\Delta\lambda$ . The consequence is the appearance of energy at the dither frequency and at sidebands that are related to the applied ac strain signal whose frequency lies outside the loop bandwidth. On the other hand, when the system is locked at point 1, the signal at frequency  $2\omega$  has the largest amplitude with the least sensitivity to variations in  $\Delta\lambda$  (Fig. 11). This explains why in Fig. 14 there is a strong component at frequency  $2\omega$  with no visible sidebands. These features are interesting, but important evidence gained from Fig. 14 is the absence of a workable signature

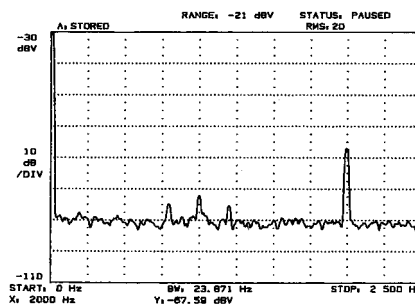


Fig. 14. Frequency spectrum of the detector output for synchronous detection at  $\omega$  and small-amplitude strain signal applied to the fiber Bragg grating (200 Hz).

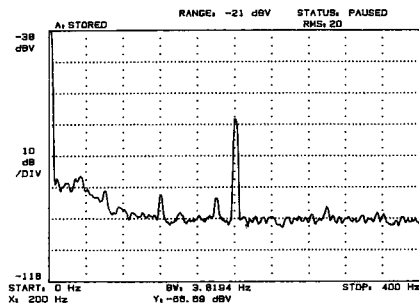


Fig. 15. Baseband frequency spectrum of the detector output for synchronous detection at  $2\omega$  when a strain signal with  $0.26\text{-}\mu\epsilon$  amplitude and 200-Hz frequency is applied to the sensing grating.

related to the applied strain signal, particularly at the baseband. Therefore the dithering technique as commonly used is not suitable for measuring small-amplitude ac signals with frequency beyond the servo bandwidth. However, as Fig. 13 demonstrates, this drawback can be bypassed by referencing the lock-in amplifier to a frequency twice the dither frequency. This is demonstrated in Fig. 15, which gives the baseband signature at the detector output corresponding to an applied sinusoidal strain signal to the sensing grating at a frequency of 200 Hz and an amplitude of  $0.26\ \mu\epsilon$ . From the observable signal-to-noise ratio and instrument bandwidth, a resolution of  $3.3\ \text{ne}/\sqrt{\text{Hz}}$  can be calculated. This value, as discussed above, is mainly determined by the system noise level, laser-mode power, and Bragg grating characteristics (reflectivity and bandwidth).

The results show the effectiveness of synchronous detection at double the dither frequency to recover sensing signals that lie outside the loop bandwidth. One might ask the following at this point: Why cannot point 2, Fig. 11, be used as an operating point to detect the signal with frequency within and beyond the bandwidth of the servo? In response to this question we refer to Eqs. (7) and (16) to see that the strength of the signals at frequencies  $\omega$  and  $2\omega$  is proportional to  $\Delta\lambda_0$  and  $\Delta\lambda_0^2$ , respectively. For a typical value of  $\Delta\lambda_0 = 0.1\ \text{nm}$  the amplitude of  $I^{2\omega}$  evaluated at zero crossing is smaller than  $I^\omega$  by a factor of  $\sim 80$  (as can be checked by comparing the scales of the bottom traces in Figs. 6 and 12). Also, the noise level with synchronous detection at  $2\omega$  is larger because the useful signal goes through the process of double differentiation compared with single differentiation for synchronous detection at  $\omega$ . These features have obvious implications in terms of achievable signal-to-noise ratios. Therefore, for signals within the loop bandwidth, optimum measurements may be made when the lock-in is referenced to the dither frequency, and for measurands with frequencies outside the loop bandwidth, twice the dither frequency is a better choice for lock-in reference.

## 5. Conclusions

Theoretical analysis and experimental results of a dithering technique applied to the demodulation of

fiber Bragg grating sensors illuminated with a low-cost multimode laser diode have been presented. The ineffectiveness of a conventional dither approach to the detection of small ac signals that lie outside the loop bandwidth has been shown, and an alternative solution based on synchronous detection at twice the dither frequency has been proposed.

L. A. Ferreira acknowledges financial support from Programa PRAXIS XXI. This research was in part supported by National Science Foundation grant DMI-9413966. The authors acknowledge theoretical insights provided by E. J. S. Lage, Departamento de Física da Faculdade de Ciências da Universidade do Porto.

## References

1. K. O. Hill and G. Meltz, "Fiber Bragg grating technology fundamentals and overview," *J. Lightwave Technol.* **15**, 1263–1276 (1997).
2. Y. J. Rao, "In-fiber Bragg gratings," *Meas. Sci. Technol.* **8**, 355–375 (1997).
3. A. D. Kersey, M. A. Davis, H. J. Patrick, M. LeBlanc, K. P. Koo, C. G. Askins, M. A. Putnam, and E. J. Frieble, "Fiber grating sensors," *J. Lightwave Technol.* **15**, 1442–1463 (1997).
4. E. Udd, ed., *Fiber Optic Smart Structures* (Wiley, New York, 1995).
5. A. D. Kersey, T. A. Berkoff, and W. W. Morey, "High resolution fiber-grating based strain sensor with interferometric wavelength shift detection," *Electron. Lett.* **28**, 236–238 (1992).
6. S. M. Melle, K. Liu, and R. M. Measures, "Practical fiber-optic Bragg grating strain gauge system," *Appl. Opt.* **32**, 3601–3609 (1993).
7. M. A. Davis and A. D. Kersey, "All-fiber Bragg grating strain-sensor demodulation technique using a wavelength division coupler," *Electron. Lett.* **30**, 75–77 (1994).
8. L. A. Ferreira and J. L. Santos, "Demodulation scheme for fiber Bragg sensors based on source spectral characteristics," *Pure Appl. Opt.* **5**, 257–261 (1996).
9. T. Coroy and R. M. Measures, "Active wavelength demodulation of a Bragg grating fiber optic strain sensor using a quantum well electroabsorption filtering detector," *Electron. Lett.* **32**, 1811–1812 (1996).
10. A. D. Kersey, M. A. Davis, and T. Tsai, "Fiber optic Bragg grating strain sensor with direct reflectometric interrogation," in *Proceedings of the Eleventh International Conference on Optical Fiber Sensors* (Japan Society of Applied Physics, Tokyo, Japan, 1996), pp. 634–637.
11. A. D. Kersey, T. A. Berkoff, and W. W. Morey, "Multiplexed fiber Bragg grating strain-sensor system with a fiber Fabry-Pérot wavelength filter," *Opt. Lett.* **18**, 1370–1372 (1993).
12. D. A. Jackson, A. B. Lobo Ribeiro, L. Reekie, and J. L. Archambault, "Simple multiplexing scheme for a fiber-optic grating sensor network," *Opt. Lett.* **18**, 1192–1194 (1993).
13. A. B. Lobo Ribeiro, L. A. Ferreira, M. Tsvetkov, and J. L. Santos, "All-fiber interrogation technique for fiber Bragg sensors using a biconical fiber filter," *Electron. Lett.* **32**, 382–383 (1996).
14. A. D. Kersey and W. W. Morey, "Multiplexed Bragg grating fiber-laser strain sensor system with mode-locked interrogation," *Electron. Lett.* **29**, 112–114 (1993).
15. S. M. Melle, A. T. Alavie, S. Karr, T. Coroy, K. Liu, and R. M. Measures, "A Bragg grating-tuned fiber laser strain sensor system," *IEEE Photon. Technol. Lett.* **5**, 263–266 (1993).
16. M. A. Davis and A. D. Kersey, "Application of a fiber Fourier transformer spectrometer to the detection of wavelength-

- encoded signals from Bragg grating sensors," *J. Lightwave Technol.* **13**, 1289–1295 (1995).
17. D. A. Flavin, R. McBride, and J. D. C. Jones, "Short optical path scan interferometric interrogation of a fiber Bragg grating embedded in a composite," *Electron. Lett.* **33**, 319–321 (1997).
  18. M. G. Xu, H. Geiger, J. L. Archambault, L. Reekie, and J. P. Dakin, "Novel interrogation system for fiber Bragg grating sensors using an acousto-optic tunable filter," *Electron. Lett.* **29**, 1510–1512 (1993).
  19. M. G. Xu, H. Geiger, and J. P. Dakin, "Modeling and performance analysis of a fiber Bragg grating interrogation system using an acousto-optic tunable filter," *J. Lightwave Technol.* **14**, 391–396 (1996).
  20. F. M. Araújo, L. A. Ferreira, J. L. Santos, and F. Farahi, "Demodulation scheme for fiber Bragg grating sensors based on active control of the spectral response of a wavelength division multiplexer," *Appl. Opt.* **37**, 7940–7946 (1998).
  21. D. R. Hjelm, L. Bjerkan, S. Neegard, J. S. Rambech, and J. V. Aarsnes, "Application of Bragg grating sensors in the characterization of scaled marine vehicle models," *Appl. Opt.* **36**, 328–336 (1997).
  22. B. Lissak, A. Arie, and M. Tur, "High resolution strain sensing by locking lasers to fiber-Bragg gratings," in *European Workshop on Optical Fiber Sensors*, B. Culshaw and J. D. C. Jones, eds., Proc. SPIE **3483**, 250–254 (1998).
  23. L. A. Ferreira, E. V. Diatzikis, J. L. Santos, and F. Farahi, "Frequency-modulated multimode laser diode for fiber Bragg grating sensors," *J. Lightwave Technol.* **16**, 1620–1630 (1998).
  24. P. J. Moreira, L. A. Ferreira, J. L. Santos, and F. Farahi, "Extended range interrogation scheme for fiber Bragg grating sensors using a multimode laser diode," in *European Workshop on Optical Fiber Sensors*, B. Culshaw and J. D. C. Jones, eds., Proc. SPIE **3483**, 278–282 (1998).
  25. E. I. Moses and C. L. Tang, "High-sensitivity laser wavelength-modulation spectroscopy," *Opt. Lett.* **1**, 115–117 (1977).
  26. G. C. Bjorklund, "Frequency-modulation spectroscopy: a new method for measuring weak absorptions and dispersions," *Opt. Lett.* **5**, 15–17 (1980).
  27. A. D. Kersey, "Interrogation and multiplexing techniques for fiber Bragg grating strain sensors," in *Distributed and Multiplexed Fiber Optic Sensors III*, J. P. Dakin and A. D. Kersey, eds., Proc. SPIE **2071**, 30–48 (1993).
  28. T. E. Clark, E. Udd, and J. A. Eck, "Demodulation of Bragg grating sensors," in *Fiber Optic Physical Sensors in Manufacturing and Transportation*, J. W. Berthold III, R. O. Claus, M. A. Marcus, and R. S. Rogowski, eds., Proc. SPIE **2072**, 274–282 (1993).
  29. A. B. Lobo Ribeiro, L. A. Ferreira, J. L. Santos, and D. A. Jackson, "Analysis of the reflective-matched fiber Bragg grating sensing interrogation scheme," *Appl. Opt.* **36**, 934–939 (1997).